Motile micro-organism based trihybrid nanofluid flow with an application of magnetic effect across a slender stretching sheet: Numerical approach

Cite as: AIP Advances 13, 035237 (2023); doi: 10.1063/5.0144191
Submitted: 28 January 2023 • Accepted: 5 March 2023 •
Published Online: 27 March 2023

Fayza Abdel Aziz Elsebaee,[1,2] Muhammad Bilal,[3] Samy Refahy Mahmoud,[4] Mohammed Balubaid,[5] Muhammad Shuaib,[6] Joshua K. K. Asamoah,[7,a)] and Aatif Ali[8]

AFFILIATIONS

[1] Mathematics Department, Faculty of Science, Helwan University, Cairo, Egypt
[2] Department of Mathematics, College of Science and Arts, Alasyah, Qassim University, Buraydah 52571, Saudi Arabia
[3] Sheikh Taimur Academic Block-II, Department of Mathematics, University of Peshawar, 25120 Khyber Pakhtunkhwa, Pakistan
[4] GRC Department, Applied College, King Abdulaziz University, Jeddah, Saudi Arabia
[5] Department of Industrial Engineering, Faculty of Engineering, King Abdulaziz University, Jeddah, Saudi Arabia
[6] Department of Mathematics, City University of Science and Information Technology, Peshawar, Pakistan
[7] Department of Mathematics, Kwame Nkrumah University of Science and Technology, Kumasi, Ghana
[8] Department of Mathematics, Abdul Wali Khan University, Mardan 23200, Pakistan

[a)] Author to whom correspondence should be addressed: jkkasamoah@knust.edu.gh

ABSTRACT

The steady magnetohydrodynamic ternary hybrid nanofluid flow over a slender surface under the effects of activation energy, Hall current, chemical reactions, and a heat source has been reported. A numerical model is developed to increase the rate of energy transfer and boost the efficiency and outcome of heat energy dissemination for a diverse range of biological applications and commercial uses. The rheological properties and thermal conductivity of the base fluids are improved by framing an accurate combination of nanoparticles (NPs). The ternary hybrid nanofluid has been prepared, in the current analysis, by the dispersion of magnesium oxide, titanium dioxide (TiO_2), and cobalt ferrite ($CoFe_2O_4$) NPs in the base fluid. The physical phenomena have been expressed in the form of a system of nonlinear PDEs, which are degraded to a dimensionless system of ODEs through the similarity replacement and numerically solved by employing the MATLAB software package bvp4c. The graphical and tabular results are estimated for velocity, mass, and energy curves vs distinct physical factors. It has been noticed that the variation in the magnetic effect enhances the energy profile while the increasing number of ternary nanocomposites (MgO, TiO_2, and $CoFe_2O_4$) in water lowers the energy curve. Furthermore, the effect of both Lewis and Peclet numbers weakens the motile microbe's profile.

I. INTRODUCTION

The analysis of nanoliquid flow across a slender stretching sheet has abundant uses in several sectors of manufacturing and engineering, such as in polymer manufacturing, aerodynamics, extrusion of polymer, glass and fiber production, and metallic furnaces.[1] Hayat *et al.*[2] evaluated the non-linear dual stratified impact of the magnetohydrodynamic (MHD) flow of nanoliquid across an enclosed surface. It was found that the upshot velocity ratio factor results in the augmentation of the velocity field. Sharma *et al.*[3] addressed the variable physical characteristics of viscoelastic fluid flow past an slender elongating surface, such as specific viscosity and thermal conductivity. Hou *et al.*[4] calculated the flow of a hybridized fluid along a slender substrate. It was discovered that advanced values of the Hartmann number and the wall thickness factor generate a retardation impact, resulting in a decrease in fluid velocity for SWCNT

and MWCNT hybrid nanofluid. Bilal *et al.*[5] scrutinized the flow features of mixed convection, Darcy nanocomposite flow along a porous slender stretched surface. The thermal energy outline is magnified by increasing the electric current, and the mass transmission coefficient increases with the influence of potential energy. Elattar *et al.*[6] documented the flow of a consistent electrically charged nanofluid flow over an elongating slender texture in the presence of varying magnetic effects, energy dissipation, and chemical reactions. The influence of the Hall current was observed to improve the axial streamlines. Saravana *et al.*[7] documented the MHD Casson fluid motion across an extended sheet and evaluated the results of Sherwood and Nusselt numbers. Murtaza *et al.*[8] observed the stream of second-grade nanoliquid across flexible substrates in a Riga plate with varying thicknesses and determined that the characteristics of the buoyancy forces exhibit an adversarial behavior on the velocity contour. Siddique *et al.*[9] reviewed the effect of multiple slips on the MHD bioconvection of a hydromagnetic-based nanoliquid along a permeable medium due to an enlarging plate. It was discovered that increasing the porosity and magnetic factors enhances the intensity of the skin friction. Recently, many researchers have studied the fluid flow across a slender extending surface.[10–13]

Hybrid nanofluid and ternary hybrid nanofluid are advanced types of nanocomposite-based fluid, which perform well in energy transmission. Solar energy, heat converters, heat pumps, automobile engineering, electrical coolers, generators, emitting radiation systems, transmitters, biotechnology, and ship manufacturing are a few sectors where hybrid nanofluids are applicable.[14–16] Sundar *et al.*[17] assessed the heat entropy, energy efficiency, and frictional entropy of a graphene oxide-based hybrid nanoliquid flow through a capillary tube and laminar flow. Xuan *et al.*[18] experimentally examined the thermal efficiency of the TiO_2–Al_2O_3–Cu/water trihybrid nanoliquid. Economic findings indicated that the most effective work liquids in the turbulent and laminar flow are TiO_2–Cu–Al_2O_3/water trihybrid nanoliquids with 1 and 0.7 vol. %. Bilal *et al.*[19] revealed the characteristics of electroviscous, trihybrid nanoliquid containing TiO_2, Al_2O_3, and SiO_2 nanoparticles (NPs) flowing through simultaneous infinite sheets. The energy and velocity transit rates are observed to increase with the addition of ternary NPs to conventional fluids. Animasaun *et al.*[20] defined the effects of magnetic flux on the water-based ternary hybrid nanofluid transmitting silver, aluminum, and aluminum oxide nanomaterials of different patterns on a flat plane reflect. Fattahi *et al.*[21] used a trihybrid nanoliquid (Fe_3O_4-sAl_2O_3–ZnO) to quantitatively assess a solar collector with a surface covering. It was discovered that such a coating could reduce the drag coefficient by about 45% whereas only a minor decrease in the Nusselt number (4.5%) is observed. Zahan *et al.*[22] investigated the performance of ternary-nano-particulates [zinc (Zn), silver (Ag), and cobalt (Co)] through a converging–diverging (CD) injector. It was discovered that the Ag–Co–Zn nanoliquid has the maximum heat transition rate. Sarada *et al.*[23] analyzed the thermal convection boundary layer circulation of a trihybrid nanoliquid (CNT–silver/water) flow across a contoured shrinking sheet with chemical potential. Xiu *et al.*[24] studied the energy maintenance and energy distribution regulation using a water-based ternary nanoliquid (Al, MgO, and TiO_2) on an elongating wedge substrate. Goud *et al.*[25] investigated the thermodynamic variability in a joinery fin under slip conditions with trihybrid nanoliquid, taking the humidity ratio and temperature differences as driving pressures in mass and heat mechanisms. Adnan and Ashraf[26] observed trihybrid nanofluids (CuO–Cu–Al_2O_3/H_2O) for thermal energy storage with the innovative impact of convective heating as well as consistent magnetic field and deduced that all these fluids are indeed very valuable for commercial operations, particularly detoxification, or where mega heat transfer is necessary to achieve the workflow. Revathi *et al.*[27] used the bvp4c package to quantitatively inspect the characteristics of TiO_2 nanoparticles and the applicability of contaminant reactive filtered water due to bioconvection in industry sectors. Gupta *et al.*[28] evaluated the 3D magneto unsteady flow of trihybrid nanoliquid induced by a spirally enlarged infinite disk under numerous slip conditions. Recently, many researchers worked on the ternary nanofluid flow.[29–32]

Micro-organisms are mono-celled microbes that are found in all living things. Because they are much heavier than base fluids, microbes become a source of bioconvection. Oxytocic microbes that swim depict the bioconvection characteristic. The bioconvection framework is concerned with swimming cells that are connected to micro-organisms. The physical significance of bioconvection is effectively distributed in ethanol, biofuel, and a wide range of commercial and environmental systems. When gyrotactic microbes are involved, nanomaterial suspension stability is frequently found to be substantially enhanced. In recent decades, many authors have written about these captivating concepts.[33–35] Atif *et al.*[36] numerically analyzed the tangent hyperbolic nanocomposite fluid flow passing through a wedge-shaped exterior filled with gyrotactic microbes. Shukla *et al.*[37] estimated the bioconvection nanoliquid flow using the homotopy analysis method. The calculations show that increasing the magnetic force and bioconvection Rayleigh number slows the flow while increasing the radiation parameter factor accelerates it. Ali *et al.*[38] defined the impact of heat absorption and generation on the Casson nanoliquid flow comprising gyrotactic microbes, with energy and mass transmission happening through parallel plates.

We have already discussed that the ternary nanofluid flow consists of ternary nanocomposites (MgO, TiO_2, and $CoFe_2O_4$) and motile microbes have several practical applications in different sectors of engineering and biomedical sciences. However, for literature review, we have concluded that very less effort has been made so far on such types of physical phenomena under the significance of activation energy, the Hall effect, and chemical reactions. Therefore, we have numerically estimated the steady MHD ternary hybrid nanoliquid flow across a slender extending sheet under the effect of variable magnetic fields, activation energy, Hall current, chemical reactions, and a heat source. A numerical model is developed to increase the rate of energy transfer and boost the efficiency and outcome of heat energy dissemination for a diverse range of biological applications and commercial uses. The physical phenomena have been expressed in the form of a system of nonlinear partial differential equations, which are numerically solved by employing the MATLAB software package bvp4c.

II. MATHEMATICAL FORMULATION

We examined steady and incompressible 2D MHD nanofluid flow over a slender stretching sheet. The surface of the sheet is variable. In the axial (x-axis) direction, the sheet stretches with velocity $U_w(x) = U_0(x + b)^n$, while the y-axis is normal to the sheet surface,

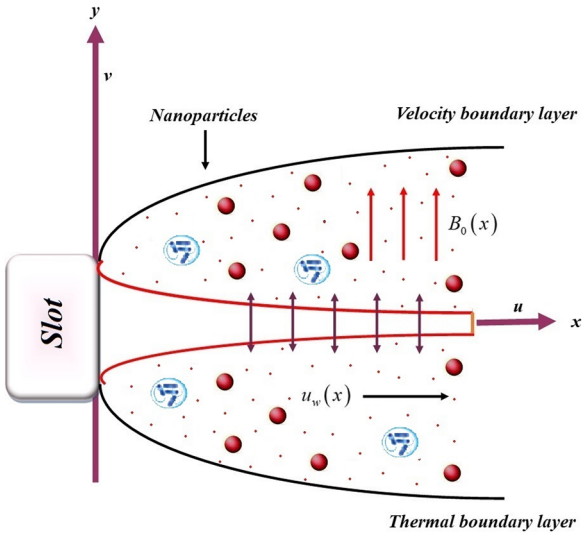

FIG. 1. Ternary hybrid nanofluid flow in a slender stretching sheet.

as depicted in Fig. 1. Here, n is the power index. The non-uniformity of the surface is assumed as $y = A(x+b)^{\frac{1-n}{2}}$, in which A is the stretching coefficient and is assumed to be negligible. The Hall current is functional for trihybrid nanoliquid circulation. Furthermore, the variable magnetic effect is applied in the y-direction. The basic governing equations are specified as[39]

$$\frac{\partial u}{\partial x} + \frac{\partial v}{\partial y} = 0, \tag{1}$$

$$\rho_{tnf}\left(u\frac{\partial u}{\partial x} + v\frac{\partial u}{\partial y}\right) = \mu_{tnf}\frac{\partial^2 u}{\partial y^2} - \frac{\sigma_{tnf}}{1+m^2}B^2(x)(u+mw), \tag{2}$$

$$\rho_{tnf}\left(u\frac{\partial w}{\partial x} + v\frac{\partial w}{\partial y}\right) = \mu_{tnf}\frac{\partial^2 w}{\partial y^2} - \frac{\sigma_{tnf}}{1+m^2}B^2(x)(mu-w), \tag{3}$$

$$\left(u\frac{\partial T}{\partial x} + v\frac{\partial T}{\partial y}\right) = \frac{k_{tnf}}{(\rho C_p)_{tnf}}\left(\frac{\partial^2 T}{\partial y^2}\right) + \tau_{tnf}\left(D_B\left(\frac{\partial T}{\partial y}\right)\frac{\partial C}{\partial y} + \frac{D_T}{T_\infty}\left(\frac{\partial T}{\partial y}\right)^2\right) + \frac{Q_0(T-T_\infty)}{(\rho C_p)_{tnf}}, \tag{4}$$

$$\left(u\frac{\partial C}{\partial x} + v\frac{\partial C}{\partial y}\right) = D_B\left(\frac{\partial^2 C}{\partial y^2}\right) + \frac{D_T}{T_\infty}\frac{\partial^2 T}{\partial y^2} - k_r^2(C-C_0)\left(\frac{T}{T_\infty}\right)^n \exp\left(-\frac{E_a}{\kappa_T}\right), \tag{5}$$

$$\left(u\frac{\partial N}{\partial x} + v\frac{\partial N}{\partial y}\right) = D_N\frac{\partial^2 N}{\partial y^2} + \frac{dW_c}{C_w - C_\infty}\left(N\frac{\partial C}{\partial y}\right). \tag{6}$$

Here, $m = \tau_e w_e$ is the Hall current, (u, v, w) are the velocity components, Q_0 is the heat source factor, E_a is the activation energy, and k_r^2 is the second-order chemical reaction.

The initial and boundary conditions are

$$\left.\begin{aligned} u = U_0(x+b)^n = U_w(x), \quad v = 0, \quad w = 0, \quad D_B\left(\frac{\partial C}{\partial y}\right) + \frac{D_T}{T_\infty}\left(\frac{\partial T}{\partial y}\right) = 0, \quad T = T_w, \quad N = N_w \ \text{at} \ y = A(x+b)^{\frac{1-n}{2}}, \\ u \to 0, \quad C \to C_\infty, \quad w \to 0, \quad T \to T_\infty, \quad N \to \infty \quad as \quad y \to \infty. \end{aligned}\right\} \tag{7}$$

The transformation variables are

$$\eta = y\sqrt{\frac{n+1}{2}\frac{U_0}{\nu_f}(x+b)^{n-1}}, \quad \psi = \sqrt{\frac{2}{n+1}\nu_f U_0(x+b)^{n+1}}f(\eta),$$
$$\hbar(\eta) = \frac{N-N_\infty}{N_w - N_\infty}, \quad \theta(\eta) = \frac{T-T_\infty}{T_w - T_\infty}, \tag{8}$$
$$w = U_0(x+b)^n h(\eta), \quad \varphi(\eta) = \frac{C-C_\infty}{C_w - C_\infty}.$$

By including Eq. (8) in Eqs. (1)–(7), we get

$$f''' + \frac{\vartheta_1}{\vartheta_2}\left(\left(ff'' - \frac{2n}{n+1}f'^2\right) - \frac{\vartheta_3}{\vartheta_1}\left(\frac{2\mathrm{M}}{(n+1)(1+m^2)}\right)f' + mg\right) = 0, \tag{9}$$

$$g'' + \frac{\vartheta_1}{\vartheta_2}\left(\left(fg' - \frac{2n}{n+1}gf'\right) - \frac{\vartheta_3}{\vartheta_1}\left(\frac{2\mathrm{M}}{(n+1)(1+m^2)}\right)mf' - g\right) = 0, \tag{10}$$

$$\theta'' + \mathrm{Pr}\,\frac{\vartheta_4}{\vartheta_5}\left(f\theta' + Nb\,\varphi'\theta' + Nt\,\theta'^2\right) + Q_1\theta = 0, \tag{11}$$

$$\varphi'' + \frac{Nt}{Nb}\theta'' + Lef\varphi' - Sc\sigma(1+\varepsilon\vartheta)^n\varphi\,\exp\left(-\frac{E}{1+\varepsilon\vartheta}\right) = 0. \tag{12}$$

$$\hbar'' + PrLbf\hbar' - Pe\left(\hbar'\phi' + \Omega\phi'' + \phi''\hbar\right) = 0. \tag{13}$$

Here,

$$\vartheta_1 = \frac{\rho_{tnf}}{\rho_f}, \quad \vartheta_2 = \frac{\mu_{tnf}}{\mu_f}, \quad \vartheta_3 = \frac{\sigma_{tnf}}{\sigma_f}, \quad \vartheta_4 = \frac{(\rho C_p)_{tnf}}{(\rho C_p)_f}, \quad \vartheta_5 = \frac{k_{tnf}}{k_f}. \tag{14}$$

The transformation conditions are

$$\left.\begin{aligned} f(\eta) = \eta\left(\frac{1-n}{1+n}\right), \quad Nb\,\varphi'(\eta) + Nt\,\theta'(\eta) = 0, \quad f'(\eta) = 1, \\ g(\eta) = 0, \quad \hbar(\eta) = 1, \quad \theta(\eta) = 1, \\ f' \to 0, \quad g \to 0, \quad \theta \to 0, \quad \varphi \to 0, \quad \hbar(\eta) \to 0 \ \ as \ \eta \to \infty. \end{aligned}\right\} \tag{15}$$

Here, $M = \frac{B_0^2\sigma_f}{\rho_f T_\infty}$ is the magnetic field, $Kr = \frac{K_c}{D_B}$ is the chemical reaction, $\Pr = \frac{\mu_f(\rho C_p)_f}{\rho_f k_f}$ is the Prandtl number, $Nt = \frac{\tau D_T(T_w - T_\infty)}{\nu_f T_\infty}$ is the thermophoresis effect, $Nb = \frac{\tau D_B C_\infty}{\nu_f}$ is the Brownian motion, $Q_1 = \frac{xQ_0}{\rho C_p}$ is the heat source, $Le = \frac{\nu_f}{D_B}$ is the Lewis number, $\delta = A\sqrt{\frac{n+1}{2}\frac{U_0}{\nu_f}}$ is the wall thickness, $Pe = \frac{dW_c}{D_N}$ is the Peclet number and $Lb = \frac{k}{D_N}$ is the Lewis number.

The skin friction, Nusselt number, and Sherwood number are

$$C_{f_x} = \frac{2\tau_{w_1}}{U_w^2\rho_f}, \quad C_{f_z} = \frac{\tau_{w_2}}{U_w^2\rho_f}, \quad Nu = \frac{q_w(x+b)}{(T_w - T_\infty)k_f}, \quad Sh = \frac{j_w(x+b)}{(C_w - C_\infty)D_B}, \tag{16}$$

where

$$\left.\begin{aligned} \tau_{w_1} &= \mu_{tnf}\left(\frac{\partial u}{\partial y}\right)_{y=A(x+b)^{\frac{1-n}{2}}}, \quad \tau_{w_2} = \mu_{tnf}\left(\frac{\partial v}{\partial y}\right)_{y=A(x+b)^{\frac{1-n}{2}}}, \\ q_w &= -k_{tnf}\left(\frac{\partial T}{\partial y}\right)_{y=A(x+b)^{\frac{1-n}{2}}}, \quad j_w = -D_B\left(\frac{\partial C}{\partial z}\right)_{y=A(x+b)^{\frac{1-n}{2}}}. \end{aligned}\right\} \tag{17}$$

The dimensionless form of Eq. (14) is

$$\left.\begin{aligned} C_{fr_x} &= \sqrt{Re_x}C_{fx} = (1-\phi_1)^{-2.5}(1-\phi_2)^{-2.5}(1-\phi_3)^{-2.5}\sqrt{2(n+1)}\,f''(0), \\ C_{fr_z} &= \sqrt{Re_x}C_{fz} = (1-\phi_1)^{-2.5}(1-\phi_2)^{-2.5}(1-\phi_3)^{-2.5}\sqrt{2(n+1)}\,g'(0), \\ Nu_r &= \frac{Nu}{\sqrt{Re_x}} = -\frac{k_{tnf}}{k_f}\sqrt{\frac{n+1}{2}}\theta'(0), \quad Sh_r = \frac{Sh}{\sqrt{Re_x}} = -\sqrt{\frac{n+1}{2}}\varphi'(0). \end{aligned}\right\} \tag{18}$$

III. NUMERICAL ESTIMATION

The obtained set of ODEs Eqs. (9)–(13) and Eq. (15) is numerically computed through the MATLAB package bvp4c as[40,41]

$$\left.\begin{aligned} -\hbar_1 = f(\eta), \quad -\hbar_3 = f''(\eta), \quad -\hbar_5 = g'(\eta), \quad -\hbar_7 = \theta'(\eta), \\ -\hbar_9 = \varphi'(\eta), \quad -\hbar_{11} = \hbar'(\eta), -\hbar_2 = f'(\eta), \quad -\hbar_4 = g(\eta), \\ -\hbar_6(\eta) = \theta(\eta), \quad -\hbar_8 = \varphi(\eta), \quad -\hbar_{10} = \hbar(\eta). \end{aligned}\right\} \tag{19}$$

By putting (19) in Eqs. (9)–(13) and Eq. (15), we get

$$\hbar\,/_3' + \frac{\vartheta_1}{\vartheta_2}\left(\left(\hbar\,/_1\hbar\,/_3 - \frac{2n}{n+1}\hbar\,/_2^2\right) - \frac{\vartheta_3}{\vartheta_1}\left(\frac{2M}{(n+1)(1+m^2)}\right)\hbar\,/_2 + m\hbar\,/_4\right) = 0, \tag{20}$$

$$\hbar\,/_5' + \frac{\vartheta_1}{\vartheta_2}\left(\left(\hbar\,/_1\hbar\,/_5 - \frac{2n}{n+1}\hbar\,/_4\hbar\,/_2\right) - \frac{\vartheta_3}{\vartheta_1}\left(\frac{2M}{(n+1)(1+m^2)}\right)m\hbar\,/_2 - \hbar\,/_4\right) = 0, \tag{21}$$

$$\hbar\,/_7' + \Pr\frac{\vartheta_4}{\vartheta_5}\left(\hbar\,/_1\hbar\,/_7 + Nb\,\hbar\,/_9\hbar\,/_7 + Nt\,\hbar\,/_7^2\right) + Q_1\hbar\,/_6 = 0, \tag{22}$$

$$\hbar\,/_9' + \frac{Nt}{Nb}\hbar\,/_7' + Le\hbar\,/_1\hbar\,/_9 - Sc\sigma(1+\varepsilon\vartheta)^n\hbar\,/_8\exp\left(-\frac{E}{1+\varepsilon\vartheta}\right) = 0, \tag{23}$$

$$-\hbar_{11}' + PrLbf - \hbar_{10} - Pe\left(-\hbar_{11} - \hbar_9 + \Omega - \hbar'_9 + -\hbar'_9 - \hbar_{10}\right) = 0. \tag{24}$$

The transformation conditions are

$$\left.\begin{aligned} \hbar\,/_1(\eta) = \eta\left(\frac{1-n}{1+n}\right), \quad Nb\,\hbar\,/_9(\eta) + Nt\,\hbar\,/_7(\eta) = 0, \\ \hbar\,/_2(\eta) = 1, \quad \hbar\,/_4(\eta) = 0, \quad \hbar\,/_6 = 1, \hbar\,/_2 \to 0, \\ \hbar\,/_4 \to 0, \quad \hbar\,/_6 \to 0, \quad \hbar\,/_8 \to 0 \ as\ \eta \to \infty. \end{aligned}\right\} \tag{25}$$

IV. RESULTS AND DISCUSSION

The physical trend and reason behind each graphical result have been described in this segment.

Velocity profile $f'(\eta)$:

Figures 2–5 illustrate the arrangement of the velocity curve $f'(\eta)$ vs parameters m, n, δ, and ϕ, respectively. Figures 2 and 3 revealed that the velocity curve $f'(\eta)$ augments with the upshot of hall current m and the power index of velocity n. Hall current (*discovered by Edwin Hall in 1879*) is the generation of the difference in voltage through a conductor that is placed transversely to the electric current and perpendicular to the magnetic field. That is why the

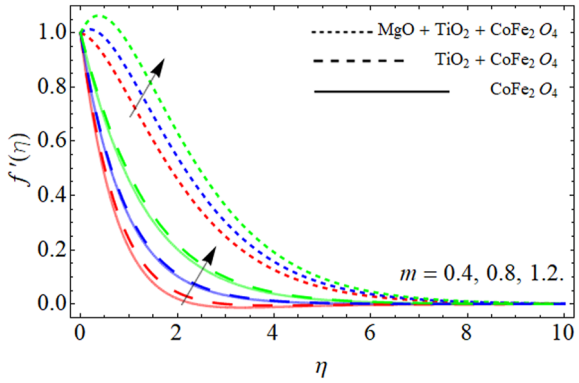

FIG. 2. Arrangement of the velocity curve $f'(\eta)$versus the Hall current *m*.

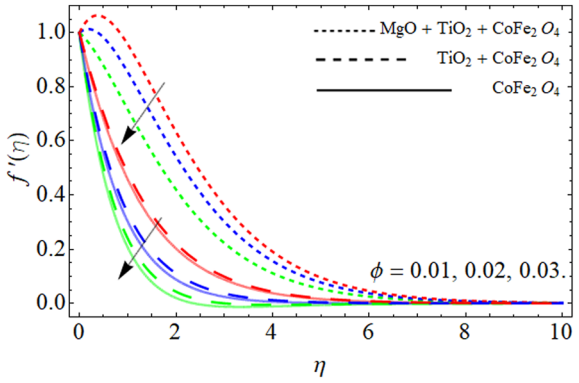

FIG. 5. Arrangement of the velocity curve $f'(\eta)$versus the volume fraction of nanoparticles ϕ.

implication of the Hall effect magnifies the velocity curve, as shown in Fig. 2.

Figures 4 and 5 demonstrate that the upshot of δ and the nanoparticle coefficient ϕ decrease the velocity outline of trihybrid nanoliquid. The increasing number of ternary nanocomposites (MgO, TiO_2, and $CoFe_2O_4$) in the base fluid makes them denser as well as improves their viscosity, which results in the decrease in the velocity curve.

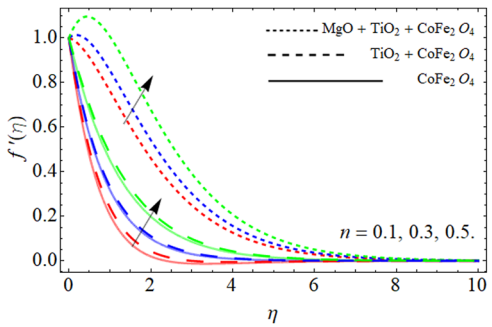

FIG. 3. Arrangement of the velocity curve $f'(\eta)$versus the velocity power index *n*.

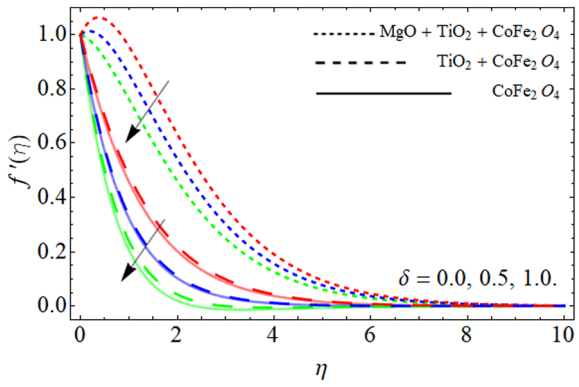

FIG. 4. Arrangement of the velocity curve $f'(\eta)$versus the wall thickness δ.

Energy profile:

Figures 6–13 show the nature of the energy curve $\theta(\eta)$ vs parameters *m*, *n*, *Q*, δ, *Nt*, *Nb*, *M*, and ϕ, respectively. Figures 6 and 7 show that the energy framework $\theta(\eta)$ augments with the outcome of *m* and *n*, respectively. Physically, the voltage difference occurs due to

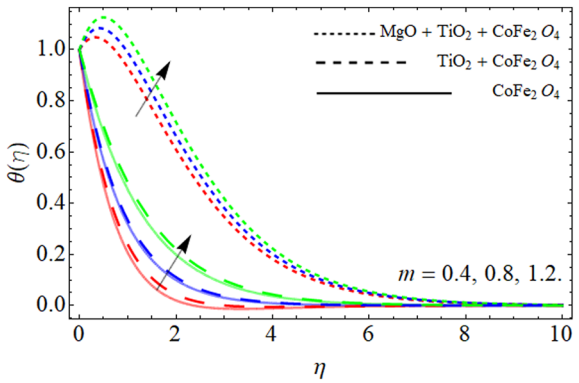

FIG. 6. Arrangement of the energy curve $\theta(\eta)$ vs the Hall current *m*.

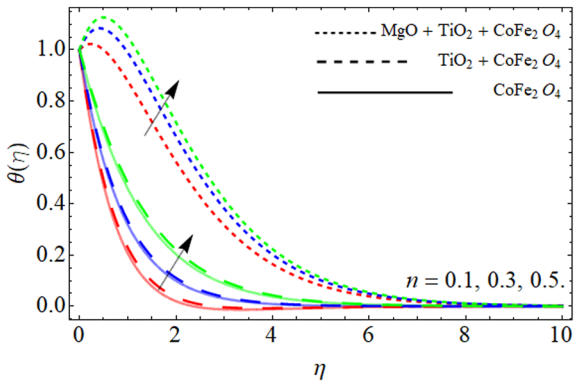

FIG. 7. Arrangement of the energy curve $\theta(\eta)$ vs the power index *n*.

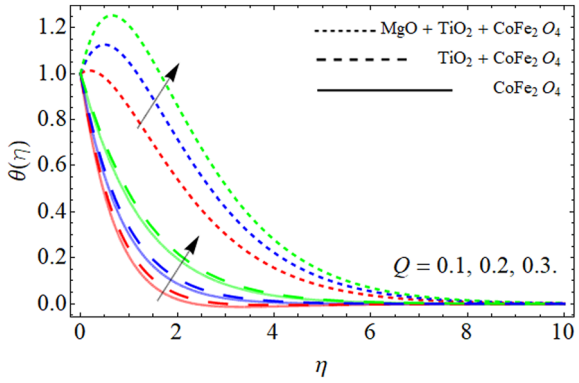

FIG. 8. Arrangement of the energy curve $\theta(\eta)$ vs the heat source *Q*.

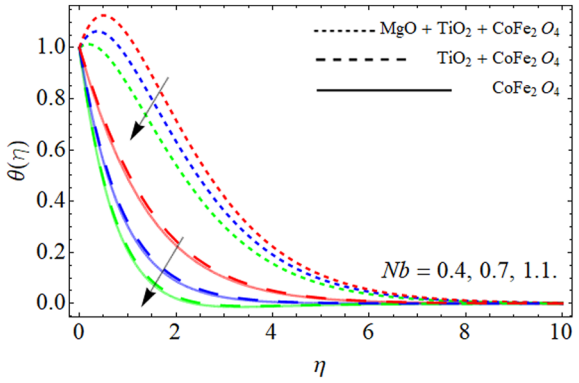

FIG. 11. Arrangement of the energy curve $\theta(\eta)$ vs the Brownian motion *Nb*.

the upshot of the Hall effect, which generates some heat and causes the elevation of the temperature curve, as shown in Fig. 6. Figures 7 and 8 show that the energy field is boosted with the significance of the heat source, which declines with the variation in δ. The influence of the heat generation term also provides additional heat to the trihybrid nanoliquid, which causes the enhancement of energy outline, as shown in Fig. 7. Physically, the variation in wall thickness generates retardation, which causes friction and enhances the energy profile (Fig. 9).

Figures 10 and 11 show the exhibition of the energy curve vs the effect of *Nb* and thermodiffusion. The influence of both parameters

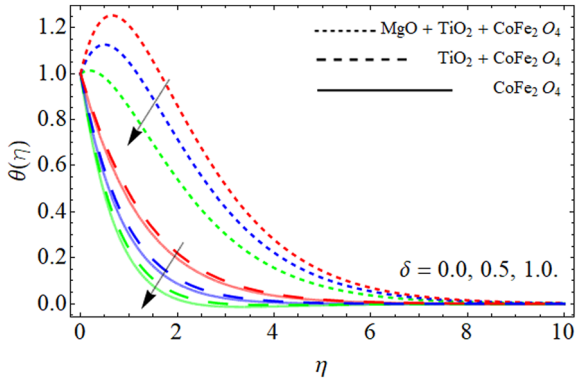

FIG. 9. Arrangement of the energy curve $\theta(\eta)$ vs the wall thickness δ.

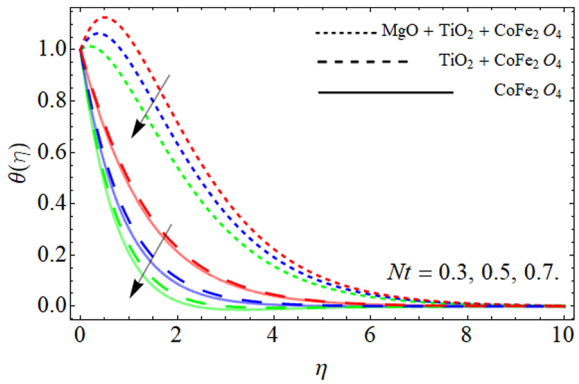

FIG. 10. Arrangement of the energy curve $\theta(\eta)$ vs the thermodiffusion *Nt*.

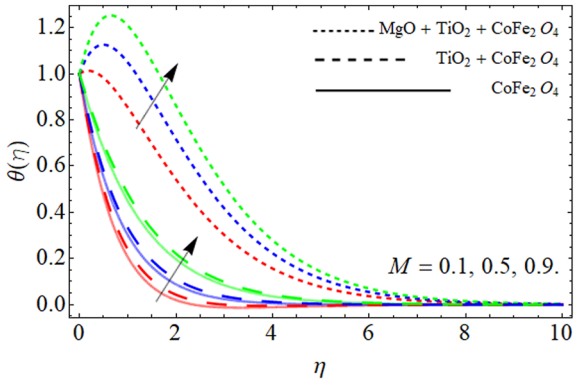

FIG. 12. Arrangement of the energy curve $\theta(\eta)$ vs the magnetic field *M*.

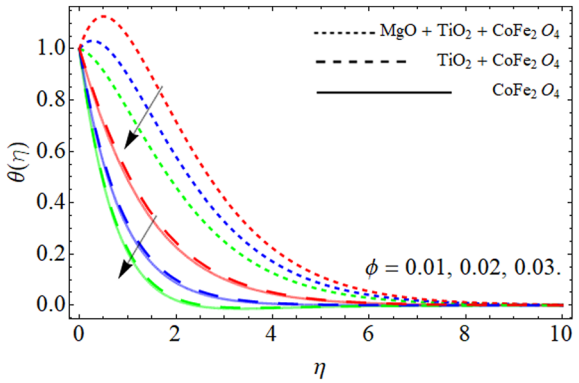

FIG. 13. Arrangement of the energy curve $\theta(\eta)$ vs the volume fraction of nanoparticles ϕ.

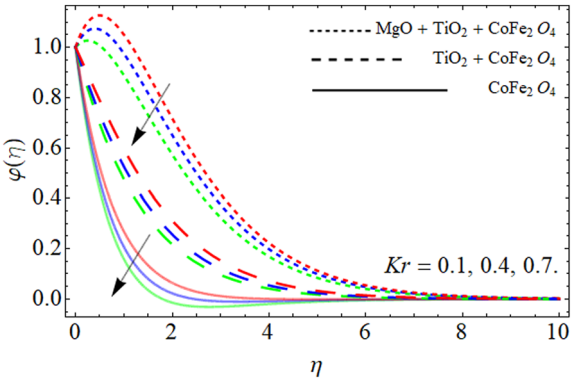

FIG. 14. Arrangement of mass $\varphi(\eta)$ outline vs the chemical reaction term *Kr*.

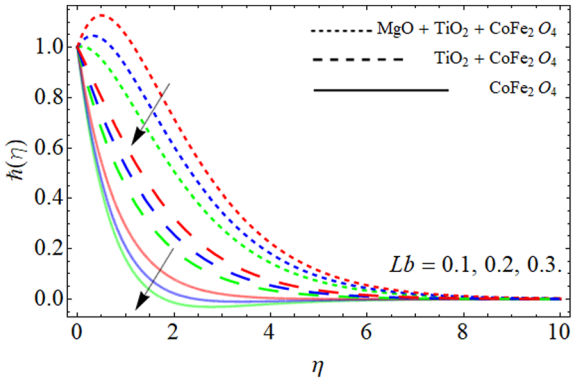

FIG. 17. Arrangement of motile microbes $\hbar(\eta)$ outline vs the *Lb*.

drops the energy curve. Consistently, the Brownian moment of particles evenly distributes the heat inside the fluid, which decreases the average temperature of the fluid [Fig. 10]. Thermophoresis is a mechanism noted in the mixing of fluid particles, where distinct nano-size particles respond differently to the applied temperature. Hence, thermodiffusion tends to interchange the heavy particles to the light molecule region and vice versa. Thus, the average temperature of trihybrid nanoliquid decreases as a result of the thermophoresis effect, as shown in Fig. 11. Figures 12 and 13 emphasize the appearance of the energy curve $\theta(\eta)$ vs M and increasing number of nanoparticles ϕ. The opposing force generated due to the magnetic impact retards the fluid motion, which sources the enhancement of the energy curve, as shown in Fig. 12. As discussed earlier, the increasing number of ternary nanocomposites (MgO, TiO_2, and $CoFe_2O_4$) in the base fluid makes them denser as well as improves its viscosity, which consequently declines the energy curve.

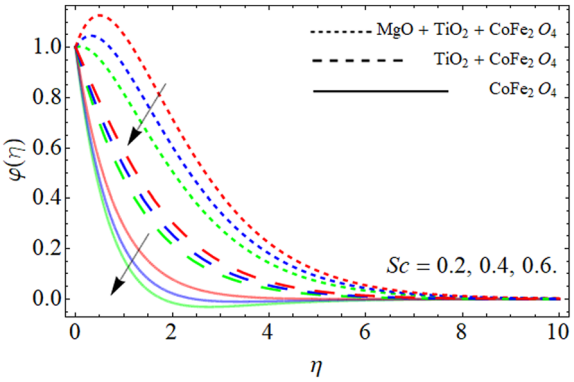

FIG. 15. Arrangement of mass $\varphi(\eta)$ outline vs the Schmidt number *Sc*.

Concentration and micro-organism profiles:

Figures 14–16 show the production of mass outline $\varphi(\eta)$ vs parameters *Kr*, *Sc*, and *E*, respectively. Figures 14 and 15 show that the mass curve declines with the variation in both *Sc* and *Kr*. The diffusion rate of fluid molecules slows down with the effect of *Kr* and *Sc*, while the viscosity of trihybrid nanoliquid is augmented, which results in a decrease in the concentration outline. Figure 16 illustrates that the upshot of activation energy boosts the rate of mass outline. The activation energy is identified as the small energy used to invigorate or stimulate fluid atoms and trihybrid nanocomposites

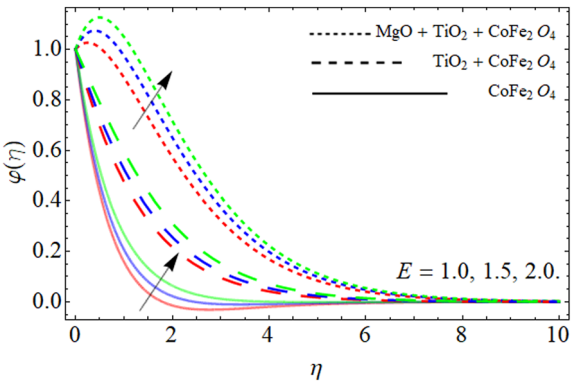

FIG. 16. Arrangement of mass $\varphi(\eta)$ outline vs the activation energy *E*.

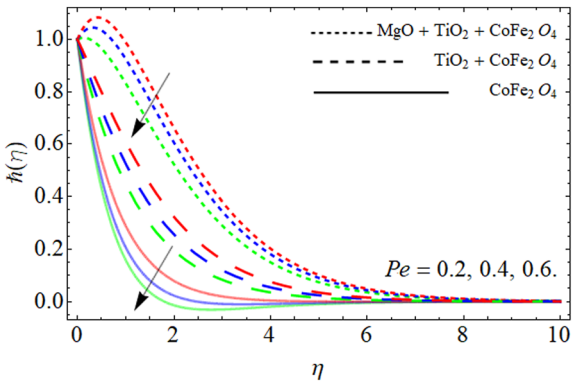

FIG. 18. Arrangement of motile microbes $\hbar(\eta)$ outline vs the Peclet number *Pe*.

Table I. The experimental values of TiO_2, $CoFe_2O_4$, MgO, and water.[6]

Base fluid and Nanoparticles	ρ (kg/m^3)	k (W/mK)	Cp (j/kg K)	σ (S/m)	$\beta \times 10^5 (K^{-1})$
Pure water, H_2O	997.1	0.613	4179	0.05	21
Magnesium oxide, MgO	3560	45	955	1.42×10^{-3}	1.26
Titanium dioxide, TiO_2	4250	8.9538	686.2	2.38×10^6	0.9
Cobalt ferrite, $CoFe_2O_4$	4907	3.7	700	5.51×10^9	⋯

TABLE II. The physical model for trihybrid nanoliquid.[6]

Viscosity	$\frac{\mu_{tnf}}{\mu_f} = \frac{1}{(1-\phi_{MgO})^{2.5}(1-\phi_{TiO_2})^{2.5}(1-\phi_{CoFe_2O_4})^{2.5}}$
Density	$\frac{\rho_{tnf}}{\rho_f} = (1-\phi_{TiO_2})\left[(1-\phi_{TiO_2})\left\{(1-\phi_{CoFe_2O_4}) + \phi_{CoFe_2O_4}\frac{\rho_{CoFe_2O_4}}{\rho_f}\right\} + \phi_{TiO_2}\frac{\rho_{TiO_2}}{\rho_f}\right] + \phi_{MgO}\frac{\rho_{MgO}}{\rho_f}$
Specific heat	$\frac{(\rho cp)_{tnf}}{(\rho cp)_f} = \phi_{MgO}\frac{(\rho cp)_{MgO}}{(\rho cp)_f} + (1-\phi_{MgO})\left[(1-\phi_{TiO_2})\left\{(1-\phi_{CoFe_2O_4}) + \phi_{CoFe_2O_4}\frac{(\rho cp)_{CoFe_2O_4}}{(\rho cp)_f}\right\} + \phi_{TiO_2}\frac{(\rho cp)_{TiO_2}}{(\rho cp)_f}\right]$
Thermal conduction	$\frac{k_{tnf}}{k_{hnf}} = \left(\frac{k_{CoFe_2O_4} + 2k_{hnf} - 2\phi_{CoFe_2O_4}(k_{hnf} - k_{CoFe_2O_4})}{k_{CoFe_2O_4} + 2k_{hnf} + \phi_{CoFe_2O_4}(k_{hnf} - k_{CoFe_2O_4})}\right)$, $\frac{k_{hnf}}{k_{nf}} = \left(\frac{k_{TiO_2} + 2k_{nf} - 2\phi_{TiO_2}(k_{nf} - k_{TiO_2})}{k_{TiO_2} + 2k_{nf} + \phi_{TiO_2}(k_{nf} - k_{TiO_2})}\right)$, $\frac{k_{nf}}{k_f} = \left(\frac{k_{MgO} + 2k_f - 2\phi_{MgO}(k_f - k_{MgO})}{k_{MgO} + 2k_f + \phi_{MgO}(k_f - k_{MgO})}\right)$,
Electrical conductivity	$\frac{\sigma_{tnf}}{\sigma_{hnf}} = \left[1 + \frac{3\left(\frac{\sigma_{CoFe_2O_4}}{\sigma_{hnf}} - 1\right)\phi_{CoFe_2O_4}}{\left(\frac{\sigma_{CoFe_2O_4}}{\sigma_{hnf}} + 2\right) - \left(\frac{\sigma_{CoFe_2O_4}}{\sigma_{hnf}} - 1\right)\phi_{CoFe_2O_4}}\right]$, $\frac{\sigma_{hnf}}{\sigma_{nf}} = \left[1 + \frac{3\left(\frac{\sigma_{TiO_2}}{\sigma_{nf}} - 1\right)\phi_{TiO_2}}{\left(\frac{\sigma_{TiO_2}}{\sigma_{nf}} + 2\right) - \left(\frac{\sigma_{TiO_2}}{\sigma_{nf}} - 1\right)\phi_{TiO_2}}\right]$, $\frac{\sigma_{nf}}{\sigma_f} = \left[1 + \frac{3\left(\frac{\sigma_{MgO}}{\sigma_f} - 1\right)\phi_{MgO}}{\left(\frac{\sigma_{MgO}}{\sigma_f} + 2\right) - \left(\frac{\sigma_{MgO}}{\sigma_f} - 1\right)\phi_{MgO}}\right]$

to contribute to a chemical change or renovation. That is why the influence of activation energy enhances the mass transmission rate, as shown in Fig. 16.

Figures 17 and 18 show the motile contour $\varphi(\eta)$ vs parameters Lb and Pe, respectively. The upshot of both Lb and Pe factors diminishes the motile microbe's curve. Physically, the density of motile microbes decreases with the influence of Lb and Pe, which results in the lessening of the motile microbe's boundary layer.

Tables I and II show the numerical values that are experimentally derived for ternary nanocomposites (MgO, TiO_2, and

TABLE III. Quantitative results for the skin friction.

			HAM	bvp4c
n	Fang *et al.*[42] $-f''(0)$	Khader *et al.*[43] $-f''(0)$	Present work $-f''(0)$	Present work $-f''(0)$
0.5	0.0000	0.000 000	0.000 000	0.000 000
1.0	0.0224	0.022 410	0.022 511	0.022 513
1.5	0.0359	0.035 871	0.035 970	0.035 987
2.0	0.0486	0.048 615	0.048 514	0.048 532
2.5	0.0550	0.055 049	0.055 248	0.055 242
3.0	0.0589	0.058 920	0.058 941	0.058 941
4.0	0.0603	0.060 329	0.060428	0.060453

TABLE IV. Quantitative results for the Nusselt number Nu_r, the Sherwood number Sh_r, and $\left(C_{f_x}, \quad C_{f_z}\right)$.

m	δ	N	C_{f_x}	C_{f_z}	Nu_r	Sh_r
0.1			−1.689 774	0.518 366	0.425 168	2.371 833
0.3			−1.286 626	0.785 571	0.459 010	2.234 450
0.5			−0.965 863	0.826 486	0.489 551	2.104 660
0.7			−0.746 347	0.865 091	0.512 454	2.006 295
0.9			−0.596 955	0.891 046	0.529 021	1.935 581
	0.1		−1.509 797	0.520 455	0.282 621	0.923 908
	0.2		−1.689 774	0.518 366	0.625 168	2.371 833
	0.3		−1.877 941	0.514 771	0.801 780	6.058 712
	0.4		−2.074 212	0.509 746	1.403 376	10.311 253
	0.5		−2.278 456	0.503 392	1.823 850	15.479 145
		0.2	−1.689 774	0.518 366	0.425 168	4.271 832
		0.4	−2.214 652	0.597 394	0.353 301	2.281 254
		0.6	−2.686 004	0.667 703	0.365 828	1.374 133
		0.8	−3.116 159	0.731 883	0.322 737	0.877 460
		1.0	−3.513 877	0.791 370	0.306 128	0.372 586

$CoFe_2O_4$) and the mathematical model used for the estimation of the results. Table III described the relative valuation of the analytic technique (HAM) and the bvp4c package. Table IV displays the arithmetical calculations of MgO, TiO_2, and $CoFe_2O_4$ ternary hybrid nanoliquid for Nu_r, Sh_r, and $\left(C_{f_x}, C_{f_z}\right)$. It is detected that the consequence of the Hall effect enhances the energy passage rate and drag force while the wall thickness factor demonstrates the opposite setup.

V. CONCLUSION

This study described the steady MHD ternary hybrid nanoliquid flow across a slender surface under the consequences of activation energy, Hall current, chemical reactions, and a heat source. The ternary HNF is prepared by the dispersion of MgO, TiO_2, and $CoFe_2O_4$ (nps) in water. The physical phenomena have been expressed in the form of a nonlinear system of PDEs. These are degraded to the dimensionless system of ODEs through the similarity replacement and numerically solved by employing the MATLAB software package bvp4c. The graphical and tabular results are estimated for velocity, mass, and energy curves vs distinct physical factors. The key findings are as follows:

- The velocity curve $f'(\eta)$ augments with the upshot of the hall current and power index of velocity n, while the influence of the wall thickness factor δ and the nanoparticle coefficient ϕ decrease the velocity outline of trihybrid nanoliquid.
- The energy outline $\theta(\eta)$ augments with the effect of Hall current, velocity index n, and heat source while it declines with the variation in the wall thickness factor δ.
- The temperature outline declines with the effect of Brownian motion and thermodiffusion.
- The variation in the magnetic effect enhances the energy profile, but the increasing number of ternary nanocomposites (MgO, TiO_2, and $CoFe_2O_4$) worsens it.
- The mass profile $\varphi(\eta)$ decays with the variation in both the Schmidt number and chemical reaction and boosts with the action of activation energy.
- The upshot of both Lb and Pe factors diminishes the motile microbe's curve.

ACKNOWLEDGMENTS

The author(s) received no specific funding for this study.

AUTHOR DECLARATIONS

Conflict of Interest

The authors have no conflicts to disclose.

Author Contributions

Fayza Abdel Aziz Elsebaee: Software (equal). **Muhammad Bilal**: Writing – original draft (equal). **Samy Refahy Mahmuod**: Validation (equal). **Mohammed Balubaid**: Conceptualization (equal). **Muhammad Shuaib**: Methodology (equal). **Joshua K. K. Asamoah**: Funding acquisition (equal); Writing – review & editing (equal). **Aatif Ali**: Writing – review & editing (lead).

DATA AVAILABILITY

The data that support the findings of this study are available within the article.

REFERENCES

[1] M. A. Mjankwi, V. G. Masanja, E. W. Mureithi, and M. N. O. James, "Unsteady MHD flow of nanofluid with variable properties over a stretching sheet in the presence of thermal radiation and chemical reaction," Int. J. Math. Math. Sci. **2019**, 7392459.

[2] T. Hayat, I. Ullah, M. Waqas, and A. Alsaedi, "MHD stratified nanofluid flow by slandering surface," Phys. Scr. **93**(11), 115701 (2018).

[3]R. P. Sharma, S. M. Ibrahim, S. R. Mishra, and S. Tinker, "Impact of dissipative heat and radiative heat on MHD viscous flow through a slandering stretching sheet with temperature-dependent variable viscosity," Heat Transfer **50**, 7568 (2021).
[4]E. Hou, F. Wang, M. N. Khan, S. Ahmad, A. Rehman, A. H. Almaliki, E.-S. M. Sherif, A. M. Galal, and M. S. Alqurashi, "Flow analysis of hybridized nanomaterial liquid flow in the existence of multiple slips and Hall current effect over a slendering stretching surface," Crystals **11**(12), 1546 (2021).
[5]M. Bilal, F. S. Alduais, H. Alrabaiah, and A. Saeed, "Numerical evaluation of Darcy Forchhemier hybrid nanofluid flow under the consequences of activation energy and second-order chemical reaction over a slender stretching sheet," Waves Random Complex Media 1–16 (2022).
[6]S. Elattar, M. M. Helmi, M. A. Elkotb, M. A. El-Shorbagy, A. Abdelrahman, M. Bilal, and A. Ali, "Computational assessment of hybrid nanofluid flow with the influence of hall current and chemical reaction over a slender stretching surface," Alexandria Eng. J. **61**(12), 10319–10331 (2022).
[7]R. Saravana, R. Hemadri Reddy, K. V. Narasimha Murthy, and O. D. Makinde, "Thermal radiation and diffusion effects in MHD Williamson and Casson fluid flows past a slendering stretching surface," Heat Transfer **51**(4), 3187–3200 (2022).
[8]S. Murtaza, P. Kumam, A. Kaewkhao, N. Khan, and Z. Ahmad, "Fractal fractional analysis of non linear electro osmotic flow with cadmium telluride nanoparticles," Sci. Rep. **12**(1), 20226 (2022).
[9]I. Siddique, U. Habib, R. Ali, S. Abdal, and N. Salamat, "Bioconvection attribution for effective thermal transportation of upper convicted Maxwell nanofluid flow due to an extending cylindrical surface," Int. Commun. Heat Mass Transfer **137**, 106239 (2022).
[10]A. Mahmood, S. Ahmed, and H. Iram, "Joule and viscous dissipation effects on MHD boundary layer flow over a stretching sheet with variable thickness," Int. J. Emerging Multidisciplinaries **1**(2), 1–10 (2022).
[11]I. Haq, M. F. Yassen, M. E Ghoneim, M. Bilal, A. Ali, and W. Weera, "Computational Study of MHD Darcy–Forchheimer hybrid nanofluid flow under the influence of chemical reaction and activation energy over a stretching surface," Symmetry **14**(9), 1759 (2022).
[12]P. K. Pattnaik, S. Mishra, and S. Jena, "Dissipative heat for the Casson fluid flow past an expanding cylindrical surface," Heat Transfer **51**(3), 2476–2487 (2022).
[13]R. S. Varun Kumar, P. Gunderi Dhananjaya, R. Naveen Kumar, R. J. Punith Gowda, and B. C. Prasannakumara, "Modeling and theoretical investigation on Casson nanofluid flow over a curved stretching surface with the influence of magnetic field and chemical reaction," Int. J. Comput. Methods Eng. Sci. Mech. **23**(1), 12–19 (2022).
[14]I. Haq, M. Bilal, N. A. Ahammad, M. E. Ghoneim, A. Ali, and W. Weera, "Mixed convection nanofluid flow with heat source and chemical reaction over an inclined irregular surface," ACS Omega **7**, 30477 (2022).
[15]T.-C. Sun, M. H. DarAssi, M. Bilal, and M. A. Khan, "The study of Darcy-Forchheimer hybrid nanofluid flow with the thermal slip and dissipation effect using parametric continuation approach over a rotating disk," Waves Random Complex Media 1–14 (2022).
[16]K. A. M. Alharbi, A. E.-S. Ahmed, M. Ould Sidi, N. A. Ahammad, A. Mohamed, M. A. El-Shorbagy, M. Bilal, and R. Marzouki, "Computational valuation of Darcy ternary-hybrid nanofluid flow across an extending cylinder with induction effects," Micromachines **13**(4), 588 (2022).
[17]L. S. Sundar, K. V. Chandra Mouli, Z. Said, and A. Sousa, "Heat transfer and second law analysis of ethylene glycol-based ternary hybrid nanofluid under laminar flow," J. Therm. Sci. Eng. Appl. **13**(5), 051021 (2021).
[18]Z. Xuan, Y. Zhai, M. Ma, Y. Li, and H. Wang, "Thermo-economic performance and sensitivity analysis of ternary hybrid nanofluids," J. Mol. Liq. **323**, 114889 (2021).
[19]M. Bilal, A. E.-S. Ahmed, R. A. El-Nabulsi, N. A. Ahammad, K. A. M. Alharbi, M. A. Elkotb, W. Anukool, and A. S. A. Zedan, "Numerical analysis of an unsteady, electroviscous, ternary hybrid nanofluid flow with chemical reaction and activation energy across parallel plates," Micromachines **13**(6), 874 (2022).
[20]I. L. Animasaun, S.-J. Yook, T. Muhammad, and A. Mathew, "Dynamics of ternary-hybrid nanofluid subject to magnetic flux density and heat source or sink on a convectively heated surface," Surfaces Interfaces **28**, 101654 (2022).
[21]A. Fattahi and N. Karimi, "Numerical simulation of the effects of superhydrophobic coating in an oval cross-sectional solar collector with a wavy absorber filled with water-based Al_2O_3-ZnO-Fe_3O_4 ternary hybrid nanofluid," Sustainable Energy Technol. Assess. **50**, 101881 (2022).
[22]I. Zahan, R. Nasrin, and S. Khatun, "Thermal performance of ternary-hybrid nanofluids through a convergent-divergent nozzle using distilled water-ethylene glycol mixtures," Int. Commun. Heat Mass Transfer **137**, 106254 (2022).
[23]K. Sarada, F. Gamaoun, A. Abdulrahman, S. O. Paramesh, R. Kumar, G. D. Prasanna, and R. P. Gowda, "Impact of exponential form of internal heat generation on water-based ternary hybrid nanofluid flow by capitalizing non-Fourier heat flux model," Case Stud. Therm. Eng. **38**, 102332 (2022).
[24]W. Xiu, I. L. Animasaun, Q. M. Al-Mdallal, A. K. Alzahrani, and T. Muhammad, "Dynamics of ternary-hybrid nanofluids due to dual stretching on wedge surfaces when volume of nanoparticles is small and large: Forced convection of water at different temperatures," Int. Commun. Heat Mass Transfer **137**, 106241 (2022).
[25]J. S. Goud, P. Srilatha, R. S. Varun Kumar, K. T. Kumar, U. Khan, Z. Raizah, H. S. Gill, and A. M. Galal, "Role of ternary hybrid nanofluid in the thermal distribution of a dovetail fin with the internal generation of heat," Case Stud. Therm. Eng. **35**, 102113 (2022).
[26]Adnan and W. Ashraf, "Thermal efficiency in hybrid (Al_2O_3-CuO/H_2O) and ternary hybrid nanofluids (Al_2O_3-CuO-Cu/H_2O) by considering the novel effects of imposed magnetic field and convective heat condition," Waves Random Complex Media 1–16 (2022).
[27]G. Revathi, I. L. Animasaun, V. S. Sajja, M. Jayachandra Babu, N. Boora, and C. S. K. Raju, "Significance of adding titanium dioxide nanoparticles to an existing distilled water conveying aluminum oxide and zinc oxide nanoparticles: Scrutinization of chemical reactive ternary-hybrid nanofluid due to bioconvection on a convectively heated surface," Nonlinear Eng. **11**(1), 241–251 (2022).
[28]G. Gupta and P. Rana, "Comparative study on Rosseland's heat flux on three-dimensional MHD stagnation-point multiple slip flow of ternary hybrid nanofluid over a stretchable rotating disk," Mathematics **10**(18), 3342 (2022).
[29]M. A. Khan, S. Bashir, N. A. Chishti, E. Bonyah, A. Dawood, and Z. Ahmad, "Effect of ambient environment and magnetic field on laser-induced cobalt plasma," AIP Adv. **13**(1), 015017 (2023).
[30]S. A. Khan, T. Hayat, and A. Alsaedi, "Thermal conductivity performance for ternary hybrid nanomaterial subject to entropy generation," Energy Rep. **8**, 9997–10005 (2022).
[31]R. Habib, T. S. Khan, Z. Ahmad, M. S. Khan, and E. Bonyah, "Two-dimensional stable lattice Boltzmann simulation of turbulent flow in wavy walled channel," AIP Adv. **13**(1), 015114 (2023).
[32]M. Ramzan, A. Saeed, P. Kumam, Z. Ahmad, M. S. Junaid, and D. Khan, "Influences of Soret and Dufour numbers on mixed convective and chemically reactive Casson fluids flow towards an inclined flat plate," Heat Transfer **51**(5), 4393–4433 (2022).
[33]E. A. Algehyne, Y. Y. Alhusayni, A. Tassaddiq, A. Saeed, and M. Bilal, "The study of nanofluid flow with motile microorganism and thermal slip condition across a vertical permeable surface," Waves Random Complex Media 1–18 (2022).
[34]Y. P. Lv, E. A. Algehyne, M. G. Alshehri, E. Alzahrani, M. Bilal, M. A. Khan, and M. Shuaib, "Numerical approach towards gyrotactic microorganisms hybrid nanoliquid flow with the hall current and magnetic field over a spinning disk," Sci. Rep. **11**(1), 1–13 (2021).
[35]Y. J. Xu, M. Bilal, Q. Al-Mdallal, M. A. Khan, and T. Muhammad, "Gyrotactic micro-organism flow of Maxwell nanofluid between two parallel plates," Sci. Rep. **11**(1), 1–13 (2021).
[36]S. M. Atif, A. H. Ganie, I. Khan, and M. Andualem, "Unsteady MHD tangent hyperbolic nanofluid past a wedge filled with gyrotactic micro-organism," Math. Problems Eng. **2022**, 4025831 (2022).
[37]N. Shukla, P. Rana, S. Kuharat, and O. A. Bég, "Non-similar radiative bioconvection nanofluid flow under oblique magnetic field with entropy generation," J. Appl. Comput. Mech. **8**(1), 206–218 (2022).

[38]F. Ali, Z. Ahmad, M. Arif, I. Khan, and K. S. Nisar, "A time fractional model of generalized Couette flow of couple stress nanofluid with heat and mass transfer: Applications in engine oil," IEEE Access **8**, 146944–146966 (2020).
[39]K. Das, S. S. Giri, and P. K. Kundu, "Influence of Hall current effect on hybrid nanofluid flow over a slender stretching sheet with zero nanoparticle flux," Heat Transfer **50**(7), 7232–7250 (2021).
[40]Z. Raizah, A. Saeed, M. Bilal, A. M. Galal, and E. Bonyah, "Parametric simulation of stagnation point flow of motile microorganism hybrid nanofluid across a circular cylinder with sinusoidal radius," Open Phys. **21**(1), 20220205 (2023).
[41]A. M. Alqahtani, M. Bilal, M. Usman, T. R. Alsenani, A. Ali, and S. R. Mahmuod, "Heat and mass transfer through MHD Darcy Forchheimer Casson hybrid nanofluid flow across an exponential stretching sheet," J. Appl. Math. Mech. e202200213 (2023).
[42]T. Fang, J. Zhang, and Y. Zhong, "Boundary layer flow over a stretching sheet with variable thickness," Appl. Math. Comput. **218**, 7241–7252 (2012).
[43]M. M. Khader and A. M. Megahed, "Boundary layer flow due to a stretching sheet with variable thickness and slip velocity," J. Appl. Mech. Tech. Phys. **56**, 241-247 (2015).